Lung squamous cell carcinoma downregulates haptoglobin expression to inhibit M2 macrophage ferroptosis via the hemoglobin-dependent CD163/HO-1 pathway

WEIJING XIE, YING-YING LIN, GUANG-HONG TAN and FENG-YING HUANG

NHC Key Laboratory of Tropical Disease Control, School of Life Sciences and Medical Technology, Hainan Medical University, Haikou, Hainan 571199, P.R. China

Received September 18, 2025; Accepted March 5, 2026

DOI: 10.3892/ol.2026.15558

Abstract. Lung squamous cell carcinoma (LUSC) is a highly malignant tumor that poses significant challenges for targeted therapy. Thus, there is a need to identify novel treatment targets. Acute-phase proteins (APPs) have been implicated in various physiological and pathophysiological processes, including cancer progression and ferroptosis. However, it remains unclear whether APPs serve a role in the progression and ferroptosis of LUSC. In the present study, bioinformatics analysis identified a haptoglobin (*HP*) gene as a hub gene in LUSC, and its expression levels were negatively associated with patient prognosis. *HP* was notably downregulated in LUSC and significantly enriched in the ferroptosis pathway. *In vitro* experiments demonstrated that overexpression of *HP* in LUSC cells did not induce ferroptosis, as there were no significant differences in lactate dehydrogenase (LDH) release, the frequency of 7-aminoactinomycin D (7-AAD)-positive cells, Fe^{2+} levels and lipid peroxidation among the cells in the LV-Ctrl, LV-*HP*, LV-Ctrl/Hb and LV-*HP*/Hb groups. However, when M2 macrophages were cultured with conditioned medium from LUSC cells overexpressing *HP* in the presence of hemoglobin (LV-*HP*/Hb group), there was a significant induction of ferroptosis in the M2 macrophages compared with those in the LV-Ctrl, LV-*HP* and LV-Ctrl/Hb and groups. This was evidenced by the increase in LDH release, the frequency of 7-AAD-positive cells, Fe^{2+} levels, lipid peroxidation and typical ultrastructural changes observed under transmission electron microscopy. Further mechanistic investigations revealed that the anti-CD163 antibody, the HO-1 inhibitor Tin protoporphyrin IX dichloride and the Fe^{2+} chelator deferoxamine effectively alleviated M2 macrophage ferroptosis in the LV-*HP*/Hb group. These results indicated that *HP* could promote M2 macrophage ferroptosis by promoting intracellular Fe^{2+} accumulation via a hemoglobin-dependent CD163/heme oxygenase 1 pathway, indicating a potential avenue for future investigations in LUSC research.

Correspondence to: Professor Feng-Ying Huang or Professor Guang-Hong Tan, NHC Key Laboratory of Tropical Disease Control, School of Life Sciences and Medical Technology, Hainan Medical University, 3 Xueyuan Road, Haikou, Hainan 571199, P.R. China
E-mail: fyhuang16@126.com
E-mail: tanhoho@163.com

Key words: lung squamous cell carcinoma, acute-phase proteins, haptoglobin, ferroptosis, M2 macrophages

Introduction

Lung cancer is a prevalent and fatal malignancy, with non-small cell lung cancer (NSCLC) accounting for >85% of cases (1,2). Lung squamous cell carcinoma (LUSC) accounts for 25-30% of NSCLC, and presents a particularly challenging clinical scenario, with a <20% 5-year survival rate and ~400,000 annual deaths globally (3). The low frequency of epidermal growth factor receptor (EGFR) mutations in LUSC limits the efficacy of EGFR tyrosine kinase inhibitors, a standard first-line treatment for NSCLC (4). While immunotherapy has emerged as a relatively effective strategy, tumor heterogeneity, microenvironmental complexity and variable immune infiltration patterns contribute to modest response rates (5,6). Additionally, severe adverse reactions continue to impede the widespread application of immunotherapy in patients with LUSC (7). Therefore, there is an urgent need to identify novel therapeutic targets and develop innovative treatment approaches for LUSC.

Acute-phase proteins (APPs) are primarily involved in host defense and exhibit dynamic changes in expression levels during inflammatory responses, including those related to cancer such as tumor cell migration, invasion and anti-apoptotic signaling (8,9). Current literature has documented a significant decrease in APP expression during tumor development (10-12), yet the therapeutic potential of most APPs remains largely unexplored. Notably, research suggests that α-2-macroglobulin, encoded by *A2M*, could be a viable therapeutic target for NSCLC (13); however, the roles of other APPs in the progression of LUSC are still unknown. This present hypothesis that specific APPs may regulate the growth and advancement of LUSC, potentially offering a novel therapeutic avenue for managing this condition.

Ferroptosis is an iron-dependent programmed cell death mechanism that is distinct from apoptosis, necrosis and

autophagy in its morphological, biochemical and genetic characteristics (14,15). Recent studies have indicated the potential therapeutic utility of regulating ferroptosis in tumors such as hepatocellular carcinoma (16) and lung cancer (17) that have developed resistance to conventional therapies. Disruption of iron metabolism is a key mechanism that triggers ferroptosis. When intracellular iron metabolism is imbalanced, excess Fe^{2+} reacts with endogenous hydrogen peroxide via the Fenton reaction, generating substantial quantities of lipid reactive oxygen species (ROS) (18). These ROS amplify oxidative stress by activating metabolic enzymes and inducing peroxidation of polyunsaturated fatty acid phospholipids in the cell membrane (18,19). The resulting lipid peroxide production ultimately initiates ferroptosis. Consequently, both increased cellular Fe^{2+} uptake and restricted Fe^{2+} efflux can lead to iron accumulation and subsequent cell death (20).

Haptoglobin (HP) is the predominant APP in the body, with its primary biological function being the high-affinity binding of free hemoglobin to prevent toxic effects and protect the body from heme iron loss (21,22). However, its specific role in LUSC progression and ferroptosis remains largely unknown. Therefore, the present study aimed to investigate the expression and potential function of HP in LUSC, with a particular focus on its involvement in ferroptosis.

Materials and methods

Reagents and antibodies. Phorbol 12-Myristate 13-Acetate (PMA; cat. no. HY-18739), FerroOrange dye (cat. no. HY-D1913), BODIPY 581/591 C11 dye (cat. no. HY-D1301), tin protoporphyrin IX dichloride (SnPPIX, cat. no. HY-101194) and deferoxamine (DFO; cat. no. HY-B1625) were purchased from MedChemExpress. RPMI-1640 medium (cat. no. 11875093), Trypsin-EDTA (cat. no. 25200056), FBS (cat. no. A5670701), penicillin-streptomycin (cat. no. 15070063), 7-aminoactinomycin D (7-AAD, cat. no. 00-6993), PE-anti-CD206 (cat. no. 12-2069-42), APC-anti-CD163 (cat. no. 17-1639-42), Alexa Fluor 568-goat anti-rabbit IgG (cat. no. A-11011), CD163 polyclonal antibody (cat. no. PA5-109340) and formic acid (cat. no. 036617.36) were purchased from Thermo Fisher Scientific, Inc. Alexa Fluor 647-anti-heme oxygenase 1 (HO-1; cat. no. ab237268) was purchased from Abcam. The cytokines IL-4 (cat. no. 200-04-5UG) and IL-13 (cat. no. 200-13-10UG) were purchased from PeproTech Inc. (Thermo Fisher Scientific, Inc.). Hb (cat. no. CSB-NP002401h) was purchased from Cusabio Technology LLC.

Bioinformatics analysis and visualization. The Gene Expression Profiling Interactive Analysis (GEPIA) database (gepia.cancer-pku.cn) was used to examine the correlation between the expression levels of *ALB*, *A2M*, *LTF*, *IL6*, *HP*, *CP*, *APOA1* and *SERPINA1* and the prognosis of patients with LUSC based on data from The Cancer Genome Atlas (TCGA; portal.gdc.cancer.gov). Additionally, pan-cancer analysis was performed on the *HP* gene. Differentially expressed genes (DEGs) between LUSC and normal lung tissues were analyzed using TCGA and Genotype-Tissue Expression data, along with a comparison of *HP* expression between tumor and normal tissues. A GeneCards database (genecards.org) search for 'acute phase proteins' yielded 107 APP genes with relevance scores ≥1. The R package intersect function (version 1.2.0; CRAN.R-project.org/package=dplyr) was used to analyze the intersection between LUSC DEGs and APP genes. Gene interactions were examined using the STRING database (cn.string-db.org), focusing on the top 481 genes interacting with *HP*. Key node genes were identified using the cytoHubba plugin (version 0.1; Institute of Information Science at Academia Sinica) with six topological network algorithms [Maximal Clique Centrality (MCC), Maximum Neighborhood Component (MNC), radiality, closeness, Edge Percolated Component (EPC) and degree] in Cytoscape software (version 3.9.0; Cytoscape Consortium). Pearson tests in the LinkedOmics database (linkedomics.org) were performed on LUSC samples from TCGA to statistically analyze *HP*-associated genes, identifying 3,763 genes with a false discovery rate (FDR) <0.001. Using the intersect function from the R package, the intersection between *HP*-associated genes and *HP*-interacting genes was assessed. The enrichGO and enrichKEGG functions (version 4.18.4; bioconductor.org/packages/release/bioc/html/clusterProfiler.html) in R (version 4.2.1; R Core Team) were used to determine the Gene Ontology (GO) terms and perform Kyoto Encyclopedia of Genes and Genomes (KEGG) pathway enrichment analysis associated with the *HP* gene in LUSC. Ferroptosis-related genes were obtained from the KEGG database (genome.jp/kegg). For GO analysis, significance was defined as q-value <0.001 for BP and q-value <0.01 for CC and MF after Benjamini-Hochberg correction, while for KEGG analysis, a q-value <0.05 was considered significant. The LUSC datasets GSE191881 and GSE74706 from Gene Expression Omnibus (GEO; ncbi.nlm.nih.gov/geo), along with gene expression profiles of LUSC tissues and normal lung tissues from TCGA, and relative HP protein expression levels from The Human Protein Atlas database (version 25.0; proteinatlas.org/ENSG00000257017-HP/cancer/lung+cancer#cptac_lung_sqcc), were obtained for analysis. The LM22 gene signature matrix, which contains characteristic genes of M2 macrophages, was obtained from a previous study (23). The infiltration levels of M2 macrophages in LUSC tissues were evaluated using the CIBERSORT (https://github.com/Moonerss/CIBERSORT; accessed in September 2025) algorithm.

Venn diagrams were drawn using the VennDetail function (version 1.26.0; bioconductor.org/packages/VennDetail) in R, along with the Venn function (version 1.12; CRAN.R-project.org/package=venn) and ggvenn function (version 0.1.19; CRAN.R-project.org/package=ggvenn). GO and KEGG enrichment circle plots were generated using OmicShare Tools (omicshare.com; accessed in September 2025).

Cell lines and cell culture. Human normal lung epithelial cells BEAS-2B were obtained from Jennio Biotech Co., Ltd. and were verified using STR analysis. The lung squamous cell lines (NCI-H226, NCI-H520, NCI-H1703 and NCI-H2170) and the human pro-monocyte cell line THP-1 were purchased from Procell Life Science & Technology Co., Ltd. and were verified using STR analysis. BEAS-2B cells were cultured in bronchial epithelial cell-specific medium (Jennio Biotech Co.), which was already supplemented with dThe NCI-H226, NCI-H520, NCI-H1703, NCI-H2170 and THP-1 cells were cultured in RPMI-1640 (Thermo Fisher Scientific, Inc.)

medium supplemented with 1% penicillin-streptomycin and 10% FBS (Thermo Fisher Scientific, Inc.). All cells were maintained at 37˚C and 5% CO_2. THP-1 cells were differentiated into M2 macrophages as described previously (24). Briefly, THP-1 cells were treated with 150 nM Phorbol 12-Myristate 13-Acetate for 24 h, followed by culture in fresh RPMI-1640 for 24 h. The macrophages were polarized into M2 macrophages by incubating them with IL-4 (20 ng/ml) and IL-13 (20 ng/ml) for 24 h. The cells were stained with APC-anti-CD163 and PE-anti-CD206 for flow cytometry analysis using the CyFlow Cube 6 system (Sysmex Europe SE) to confirm M2 macrophage polarization.

Reverse transcription-quantitative PCR (RT-qPCR). Total RNA was extracted from BEAS-2B and LUSC cell lines (NCI-H226, NCI-H520, NCI-H1703, and NCI-H2170) using TRIzol® reagent (cat. no. 15596018CN; Thermo Fisher Scientific, Inc.) and treated with DNase I to eliminate DNA contamination. Subsequently, single-stranded cDNA was synthesized from RNA using reverse transcriptase M-MLV (cat. no. 6110B; Takara Bio, Inc.). The following primer sequences used for amplification of *HP* and *GAPDH* were as follows: *HP* forward (F), 5'-CAGCACAGTCCCCGAAAAGAA-3' and reverse; 5'-CAGTCGCATACCAGGTGTCC-3'; and *GAPDH* F, 5'-GGAGCGAGATCCCTCCAAAAT-3' and R, 5'-GGCTGTTGTCATACTTCTCATGG-3'; primers were synthesized by Takara Bio, Inc. qPCR analysis was performed using UltraSYBR Green Master Mix (cat. no. CW0957H; Jiangsu Kangwei Century Biotechnology Co., Ltd.) to measure the mRNA expression levels of *HP*. Cq values for *HP* were normalized to GAPDH, and quantitative analysis was performed using the $2^{-\Delta\Delta Cq}$ method (25). The PCR amplification conditions were based on a published report (26). The thermocycling program consisted of an initial denaturation at 95˚C for 1 min (1 cycle), followed by 40 cycles of denaturation at 95˚C for 5 sec, annealing at 60˚C for 10 sec and extension at 72˚C for 15 sec, with a final extension at 72˚C for 10 min (1 cycle). RT-qPCR analysis was performed using rTaq (Takara Bio, Inc.) in a DNA thermal cycler (Maxygen).

ELISA. HP levels in BEAS-2B and LUSC cell lines (NCI-H226, NCI-H520, NCI-H1703, and NCI-H2170) were determined using an HP assay kit (cat. no. E-EL-H6199; Wuhan Elabscience Biotechnology Co., Ltd.) according to the manufacturer's protocol. Culture supernatants from cells in the logarithmic growth phase were collected and diluted 1:10,000. The diluted test samples, standard solutions and blank diluent were added into microplate wells at 100 μl per well, and then incubated at 37˚C for 90 min. The intracellular fluid was then discarded, and 100 μl biotinylated antibody working solution was added to each well, followed by incubation at 37˚C for 60 min. The plate was then washed three times with detergent, and 100 μl HRP enzyme conjugate working solution was added to each well. The plate was incubated at 37˚C for 30 min, followed by five washes. Then, 90 μl 3,3',5,5'-Tetramethylbenzidine substrate solution was added to each well and incubated at 37˚C in the dark for 15 min before adding 50 μl stop solution to terminate the reaction. Finally, the optical density (OD) value of each well was measured at a wavelength of 450 nm using an ELISA reader (ELX 808IU; Omega Bio-Tek, Inc.), and protein concentrations were calculated using a standard curve.

Lentiviral infection. Recombinant lentiviral vectors overexpressing *HP* (LV-*HP*; GV492-Ubc-HP-3FLAG) and a control vector (LV-Ctrl; GV492-Ubc-MCS-3FLAG) were designed and synthesized by Shanghai GeneChem Co., Ltd. A third-generation self-inactivating lentiviral packaging system was used. HEK293T cells (Shanghai GeneChem Co., Ltd.) were co-transfected with 20 μg of GV vector plasmid, 15 μg of pHelper 1.0 and 10 μg of pHelper 2.0 (mass ratio of 20:15:10). The transfection mixture was incubated at room temperature for 15 min and added to the cells. After 6-8 h at 37˚C, the medium was replaced. Lentiviral particles were harvested 48 h post-transfection, concentrated by ultracentrifugation at 53,000 x g for 2 h at 4˚C, and resuspended in PBS.

To establish HP overexpression cells, NCI-H226 and NCI-H520 cells were infected with LV-*HP* or LV-Ctrl (multiplicity of infection, 50). The cells were plated at a density of $5x10^4$ cells/well in a 6-well plate and cultured until reaching 30% confluence. Subsequently, the cells were infected with 200 μl lentivirus and 40 μl transfection enhancer HiTransG A for 16 h. Following this, the medium was replaced with fresh complete culture medium for further cultivation. After 72 h post-infection, the efficiency of HP overexpression was assessed in cells and culture supernatant using RT-qPCR and ELISA, respectively.

Lactate dehydrogenase release (LDH) assay. An LDH cytotoxicity assay kit (cat. no. HY-K1090; MedChemExpress) was used to assess LDH levels in the supernatant of LUSC cell lines (NCI-H226 and NCI-H520 cells) and M2 macrophages, according to the manufacturer's protocol. LUSC cells infected with LV-*HP* or LV-Ctrl at a concentration of $1x10^5$ cells/ml were seeded in a 96-well plate at 100 μl per well and incubated with or without Hb treatment for 24 h. Similarly, M2 macrophages at a concentration of $1x10^5$ cells/ml were plated in a 96-well plate at 100 μl per well and treated with or without Hb in the presence of conditioned media (CM) from LUSC cells infected with LV-*HP* or LV-Ctrl for 24 h. After washing with PBS, 20 μl 0.4 mol/l lactic acid solution, 20 μl 4 mmol/l 2-p-iodophenyl-3-p-chloronitrobenzenetetrazole solution and 20 μl reaction solution were added to the cells. The samples were incubated at room temperature for 30 min, and the OD value was measured using an ELISA reader with a detection wavelength of 492 nm and a reference wavelength of 650 nm. The fold change for each sample (including the samples in the control group) was calculated by dividing the value of each sample by the mean value of the control group.

Flow cytometry analysis. Flow cytometry was used to quantify 7-AAD-positive dead cells, intracellular Fe^{2+} and lipid peroxide levels, CD163- and CD206-double-positive cells and HO-1-expressing cells. To assess the proportion of 7-AAD-positive cells, and the levels of intracellular Fe^{2+} and lipid peroxides in NCI-H226 and NCI-H520 cells, cells infected with LV-*HP* or LV-Ctrl were seeded at a concentration of $2x10^5$ cells per well in 6-well plates, with or without the addition of Hb, and incubated at 37˚C for 24 h. To

determine the percentage of 7-AAD-positive cells, NCI-H226 and NCI-H520 cells treated as aforementioned were washed with PBS. Subsequently, the cells were resuspended in PBS containing 1 μg/ml 7-AAD (cat. no. 00-6993; Thermo Fisher Scientific, Inc.) and incubated at room temperature in the dark for 10 min. Following trypsin digestion, the cells were washed with PBS, centrifuged at 4˚C at 200 x g for 5 min to collect the cells, and the percentage of 7-AAD-positive cells was analyzed using flow cytometry. To determine the concentration of Fe^{2+}, NCI-H226 and NCI-H520 cells, treated as aforementioned, were washed with PBS and then incubated at room temperature in the dark in 1 μmol/l FerroOrange (cat. no. HY-D1913; MedChemExpress) working solution for 30 min. Subsequently, the fluorescence intensity of FerroOrange-stained cells was measured using flow cytometry. The mean fluorescence intensity of each sample was then calculated and compared with the control group. To assess lipid peroxidation levels, NCI-H226 and NCI-H520 cells were treated with LV-HP or LV-Ctrl, washed with PBS, and then incubated in the dark at room temperature with fresh culture medium containing 2 μm BODIPY581/591C11 dye (cat. no. HY-D1301; MedChemExpress) for 30 min. Following trypsin digestion, cells were washed with PBS, collected by centrifugation at 4˚C, 200 x g for 5 min, and the fluorescence intensity of BODIPY581/591C11-stained cells was measured using flow cytometry.

To identify the induction of M2 macrophages, THP-1 cells were treated with 150 nM Phorbol 12-Myristate 13-Acetate (cat. no. HY-18739; MedChemExpress) for 24 h, cultured in fresh RPMI-1640 for 24 h, and then stimulated with IL-4 (20 ng/ml; cat. no. 200-04-5UG; Thermo Fisher Scientific, Inc.) and IL-13 (20 ng/ml; cat. no. 200-13-10UG; Thermo Fisher Scientific, Inc.) for an additional 24 h, all at 37˚C. Subsequently, the cells were washed with PBS and then incubated with APC-anti-CD163 (1:500; cat. no. 17-1639-42; Thermo Fisher Scientific, Inc.) and PE-anti-CD206 (1:500; cat. no. 12-2069-42; Thermo Fisher Scientific, Inc.) at 4˚C in the dark for 30 min. Following a final wash with PBS and centrifugation, flow cytometry was used to analyze CD163- and CD206-double-positive cells. To assess the proportion of 7-AAD-positive cells and the levels of intracellular Fe^{2+} and lipid peroxides in M2 macrophages, culture supernatants from NCI-H226 and NCI-H520 cells infected with LV-*HP* or LV-Ctrl were used as CM. M2 macrophages were cultured with the CM in combination with other reagents for 24 h. Subsequently, the M2 macrophages were stained with 7-AAD, FerroOrange or BODIPY581/591C11 dyes, followed by flow cytometry analysis. To assess the expression of HO-1 in M2 macrophages, $2x10^6$ M2 macrophages were fixed in 0.25% cold paraformaldehyde (cat. no. P0099; Beyotime Biotechnology) at 4˚C for 1 h, followed by lysis with 0.1% Triton X-100 (cat. no. HFH10; Thermo Fisher Scientific, Inc.) for 10 min at room temperature in the dark. The cells were incubated with an Alexa Fluor 647-anti-HO-1 antibody (cat. no. ab237268; Abcam) at room temperature for 1 h prior to flow cytometry analysis. All flow cytometry analyses were conducted on a CyFlow Cube 6 system. FlowJo (version 10; BD Biosciences) was used to analyze the data, employing gating strategies to exclude debris and select single cells based on the forward- and side-scatter characteristics.

Transmission electron microscopy. M2 macrophages were inoculated into a 6-well plate and co-cultured with CM and Hb for 24 h. The cells were then fixed in 2.5% glutaraldehyde in PBS at 4˚C for 4 h and subjected to three 15-min washes with PBS. Post-fixation was performed using 1% OsO_4 in PBS at 4˚C for 1.5 h, followed by three additional 15-min washes with PBS. Dehydration was performed using sequential immersions in ethanol solutions (30, 50, 70 and 80%), followed by acetone solutions (90 and 95%) for 15 min each. Absolute acetone dehydration was then performed twice for 20 min each. Subsequently, the cells were incubated in a 1:1 mixture of absolute acetone and the final Spurr resin for 1 h at room temperature, followed by a 1:3 mixture for 2 h, and finally in a mixture of the final Spurr resin and absolute acetone overnight. Following embedding, ultrathin sections, sectioned at 60 nm thickness were prepared, stained and imaged using a transmission electron microscope (cat. no. H-7650; Hitachi, Ltd.).

Determination of intracellular heme content. A total of $5x10^3$ M2 macrophages per well was inoculated into a 96-well plate and co-cultured with CM and Hb, either alone or in combination with a CD163 polyclonal antibody (1:50-100; cat. no. PA5-109340; Thermo Fisher Scientific, Inc.), for 24 h. Intracellular heme content was determined following established protocols (27). Briefly, cells were washed three times with PBS, centrifuged at 200 x g for 5 min and then resuspended in 180 μl concentrated formic acid. The heme concentration of the formic acid solution was determined spectrophotometrically at 400 nm.

Statistical analysis. Experimental data were analyzed using GraphPad Prism software version 6.0 (Dotmatics). Survival curves were generated using the Kaplan-Meier method, and differences between groups were assessed by the log-rank test. Correlation analysis was performed using the Pearson correlation coefficient. A one- or two-way ANOVA with a Tukey's post hoc test was used to compare differences among multiple groups. To determine the difference between two groups, an unpaired t-test was used. All data are presented as the mean ± SD. $P<0.05$ was considered to indicate a statistically significant difference.

Results

HP is a hub APP gene in LUSC. To investigate the expression of APPs in LUSC and its correlation with prognosis, a total of 107 APP genes were initially identified with a relevance score of ≥1 from the GeneCards database (Table SI). From the GEPIA database, 5,944 DEGs were identified between LUSC tumors and normal lung tissues (Table SII). Intersection analysis revealed 46 overlapping APP and DEG genes (Fig. 1A). STRING database analysis demonstrated significant network interactions among 44 of these 46 APP genes (Fig. 1B). Using six topological network algorithms, including MCC, MNC, degree, EPC, closeness and radiality from the Cytoscape plugin cytoHubba, eight consistently top-ranked genes were identified: *ALB*, *A2M*, *LTF*, *IL6*, *HP*, *CP*, *APOA1* and *SERPINA1* (Table SIII and Fig. 1C). Among the eight genes, Kaplan-Meier survival analysis using GEPIA data showed that only *HP* (P=0.049) and *A2M* (P=0.0043) were significantly correlated

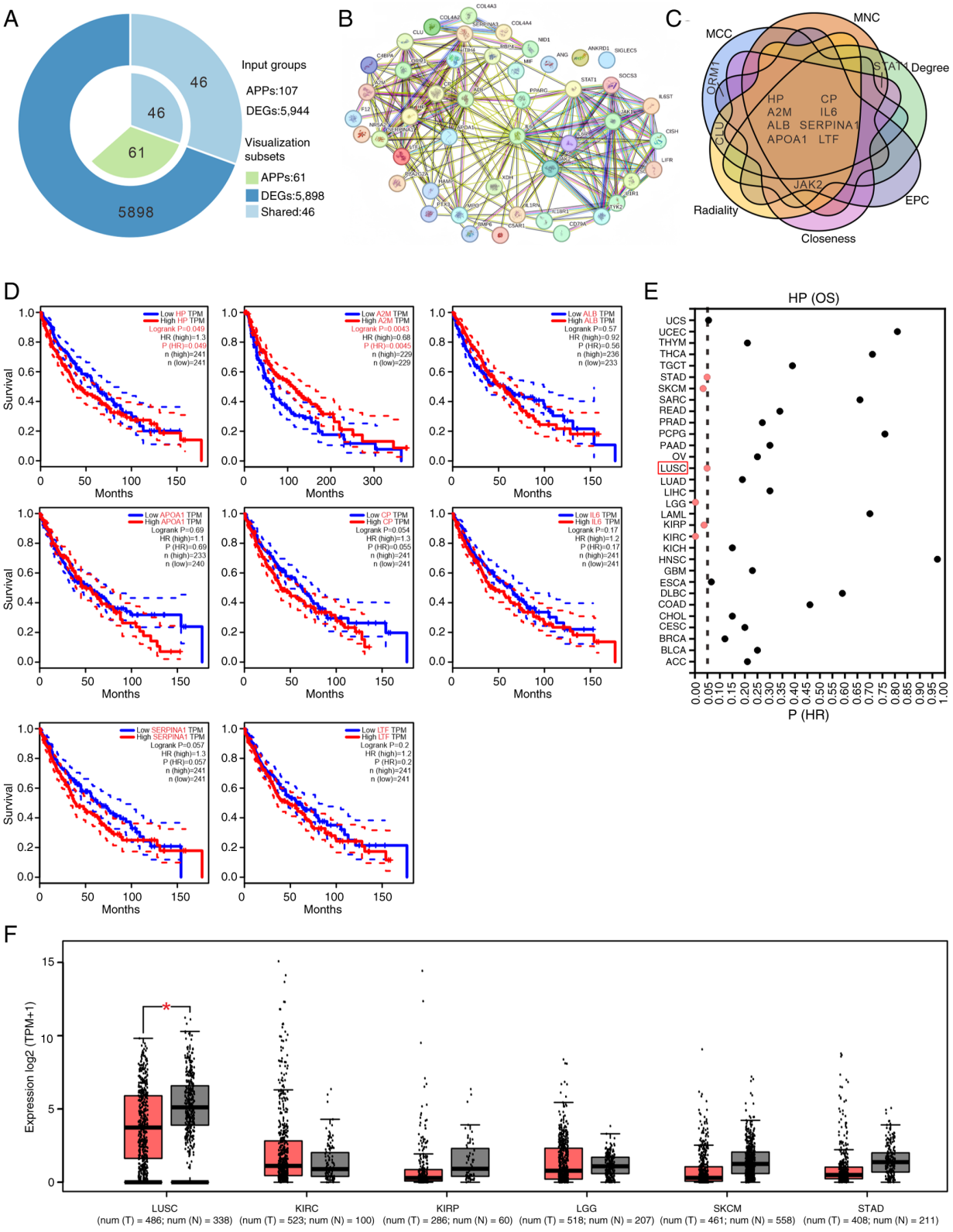

Figure 1. Identification of *HP* as a hub gene in LUSC. (A) A total of 107 acute-phase proteins with a relevance score of ≥1 were selected from the GeneCards database and intersected with 5,944 genes showing differential expression between LUSC and normal lung tissues in the GEPIA database, yielding 46 overlapping genes. (B) The 46 genes were then input into the STRING database, where 44 genes formed a significant interaction network. (C) The 44 genes within the network were then assessed using six topological network algorithms (MCC, MNC, radiality, closeness, EPC and degree) in the Cytoscape software with the cytoHubba plugin. This analysis yielded the top 10 genes ranked by each algorithm, with eight genes (*HP*, *A2M*, *ALB*, *APOA1*, *CP*, *IL6*, *SERPINA1* and *LTF*) consistently ranking highly. (D) Survival analysis conducted on the GEPIA database revealed the association between the expression levels of *HP*, *A2M*, *ALB*, *APOA1*, *CP*, *IL6*, *SERPINA1* and *LTF* and the overall survival of patients with LUSC. (E) Data analysis from the GEPIA database indicated a statistically significant association (P<0.05) between HP expression in *KIRC*, *KIRP*, *LGG*, *LUSC*, *SKCM* and *STAD* and patient OS rates. The red box is used to highlight LUSC, the focus of this study. (F) Gene expression data from the GEPIA database demonstrated a significant statistical difference in *HP* expression between LUSC tissues and normal tissues, while the changes in its expression in *KIRC*, *KIRP*, *LGG*, *SKCM* and *STAD* did not reach statistical significance. *P<0.05. *HP*, haptoglobin; LUSC, lung squamous cell carcinoma; APP, acute-phase proteins; DEG, differentially expressed genes; HR, hazard ratio; OS, overall survival; TPM, transcripts per million.

with the prognosis of patients with LUSC, while the remaining six genes did not demonstrate statistically significant prognostic associations (Fig. 1D). A previous study identified *A2M* as a potential therapeutic target for NSCLC (13). However, the specific role of the *HP* gene in predicting prognosis in NSCLC remains unexplored. Through pan-cancer analysis using the GEPIA database, it was found that *HP* was associated with the prognosis of LUSC and five other cancer types: Stomach adenocarcinoma (STAD), skin cutaneous melanoma (SKCM), brain lower grade glioma (LGG), kidney renal papillary cell carcinoma (KIRP) and kidney renal clear cell carcinoma (KIRC) (Fig. 1E). Analysis of the GEPIA database revealed a significant differential expression in *HP* gene expression in LUSC tissues compared with that of normal lung tissues, with no significant differences observed in the other five tumor types (Fig. 1F). These findings collectively indicated that *HP* was a hub gene in LUSC progression.

HP is significantly downregulated in LUSC. To investigate *HP* expression in LUSC, gene expression profiles were obtained from GEO and TCGA. Findings from GEO (Fig. 2A) and TCGA (Fig. 2B) revealed a significant downregulation of *HP* gene expression in LUSC tumor tissues compared with that of normal lung tissues. Subsequent RT-qPCR analysis of *HP* gene expression in the normal lung epithelial cell line BEAS-2B and LUSC cell lines (NCI-H226, NCI-H520, NCI-H1703, NCI-H2170) showed significant decreases in the LUSC cell lines compared with that of BEAS-2B (Fig. 2C). Examination of the Human Protein Atlas database showed a notable decrease in HP protein expression in LUSC tumor tissues compared with that of normal lung tissues (Fig. 2D). ELISA analysis also confirmed a decrease in HP protein secretion levels in LUSC cell culture supernatant compared with that from the normal lung epithelial cell line BEAS-2B (Fig. 2E). These results indicated a significant downregulation of the *HP* gene and protein in LUSC tumor tissues and cells.

HP enrichment in LUSC suggests potential involvement in the ferroptosis signaling pathway. An examination of potential signaling pathways influenced by *HP* in LUSC was conducted using TCGA data in the LinkedOmics database. The analysis identified 3,763 genes linked to *HP* with an FDR threshold of <0.001 (Table SIV). In the STRING database, by setting the maximum number of genes in the interactome to 500 and filtering for interactions with a score >0.4, 481 genes, directly or indirectly, interacted with *HP* (Table SV). When comparing the 3,763 *HP*-associated genes with the 481 interacting genes, it was found that 191 genes were both associated with and interacted with *HP* (Fig. 3A). GO enrichment analyses (Table SVI), visualized using the OmicShare platform, revealed 20 enriched GO terms across biological processes, cellular components and molecular functions (Fig. 3B, upper panel). The biological processes included lipid metabolism ('neutral lipid metabolic process', 'triglyceride metabolic process' and 'arachidonic acid secretion process') and oxidation processes ('response to oxidative stress' and 'ROS metabolic process'). Cellular component enrichment was observed in lipid components, specifically the outer mitochondrial membrane. Molecular functions included 'oxygen binding', enzyme activities ('oxidoreductase' and 'peroxidase'), 'lipoprotein lipase activator activity' and 'antioxidant activity'. The GO enrichment analysis indicated that the 191 identified genes were predominantly involved in oxidative stress responses associated with ferroptosis. This finding was corroborated by the KEGG pathway enrichment analysis, which showed a significant enrichment of these genes in the ferroptosis pathway (Fig. 3B, lower panel). Analysis of the KEGG database using the keyword 'Ferroptosis' identified 33 genes involved in the ferroptosis pathway (Table SVII). By comparing the 191 genes associated with and interacted with *HP* and the 33 ferroptosis pathway genes, four intersecting genes were identified: *HMOX1*, *SLC40A1*, *CP* and *TF* (Fig. 3C). Pearson correlation analysis revealed significant associations between *HP* and these four genes, with correlation coefficients of 0.23 ($P=2.19\times10^{-7}$), 0.31 ($P=1.47\times10^{-12}$), 0.48 ($P=3.98\times10^{-30}$) and 0.27 ($P=6.87\times10^{-10}$), respectively. These results suggested that these four genes may serve essential roles as regulators in the *HP*-induced ferroptosis pathway.

Overexpression of HP in LUSC cells does not induce ferroptosis. Given the low expression of HP in LUSC cells, lentiviral vectors were constructed to overexpress HP in the NCI-H226 and NCI-H520 LUSC cell lines. After 72 h, cells and culture supernatants were collected to quantify *HP* mRNA and protein expression using RT-qPCR and ELISA, respectively. Compared with the LV-Ctrl group, LV-*HP* infection significantly increased *HP* mRNA (Fig. 4A) and protein (Fig. 4B) expression levels, confirming the successful generation of lentiviral vectors expressing *HP* for subsequent experiments. Ferroptosis is a form of cell death triggered by iron-dependent lipid peroxidation, which increases membrane permeability (28). To study the influence of HP on membrane permeability in LUSC NCI-H226 and NCI-H520 cells, LDH release and 7-AAD assays were performed in these cells treated with or without LV-*HP* in the presence or absence of Hb. It was observed that there were no significant differences in LDH release (Fig. 4C) and 7-AAD positive cells (Fig. 4D) among the LV-Ctrl, LV-*HP*, LV-Ctrl/Hb, and LV-*HP*/Hb groups. Flow cytometry analysis showed no significant differences in intracellular Fe^{2+} (Fig. 4E) and lipid peroxides (Fig. 4F) among the cells in the LV-Ctrl, LV-*HP*, LV-Ctrl/Hb and LV-*HP*/Hb groups. Thus, it was demonstrated that the overexpression of HP did not induce ferroptosis in the LUSC cells.

CM from LUSC cells overexpressing HP leads to ferroptosis in M2 macrophages. Previous studies have elucidated the roles of *HP*, *HMOX1*, *SLC40A1*, *CP* and *TF* in regulating iron recycling in M2 macrophages, with CD163 serving as the receptor (29,30). To assess the correlation between *HP* expression and M2 macrophage abundance, LUSC samples from the TCGA database were stratified into high- and low-*HP* expression groups based on median *HP* expression levels (cut-off value, 50th percentile). An analysis of immune infiltration in the LUSC gene expression profile was then conducted to assess M2 macrophage levels in these groups. The high-*HP* expression group exhibited a significantly higher abundance of M2 macrophages compared with that of the low-*HP* expression group (Fig. S1), indicating a positive correlation between *HP* expression and M2 macrophage abundance. Furthermore, LM22 data containing characteristic genes of M2 macrophages from a previous study was

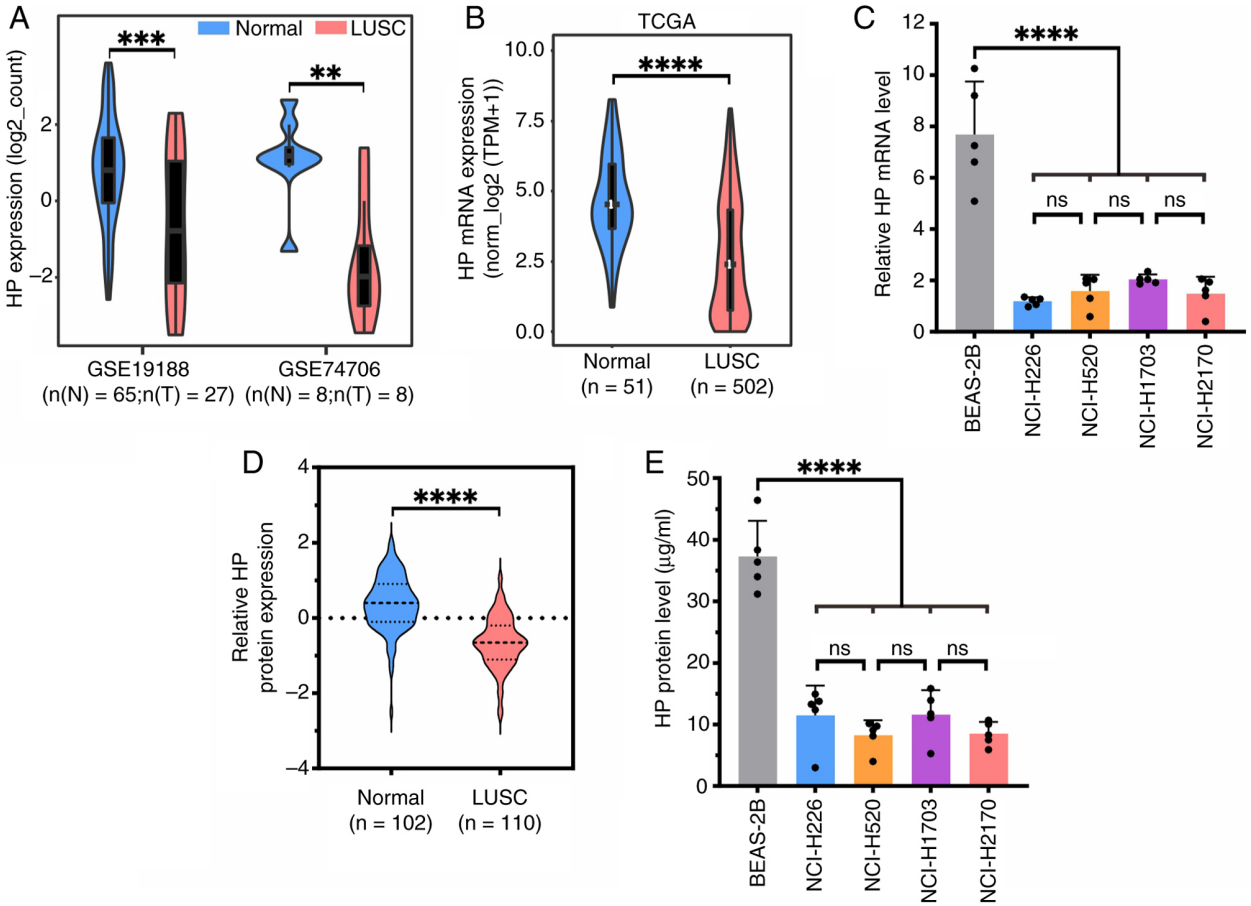

Figure 2. Significant downregulation of *HP* in LUSC. (A) The LUSC datasets GSE19188 and GSE74706 from the Gene Expression Omnibus database were examined. These datasets included 35 LUSC samples and 73 normal lung tissue samples. The objective was to evaluate *HP* gene expression in normal lung and LUSC tissues (unit: log2_count). (B) The TCGA database provided the expression profiles of the *HP* gene in normal lung and LUSC samples [unit: norm_log2(TPM+1)]. (C) Reverse transcription-quantitative PCR analysis was performed to examine *HP* mRNA expression in the normal lung epithelial cell line BEAS-2B and LUSC cell lines (NCI-H226, NCI-H520, NCI-H1703 and NCI-H2170). (D) Relative HP protein expression levels in LUSC tissues and normal lung tissues were obtained from Human Protein Atlas database. (E) ELISA was performed to assess HP secretion in the normal lung epithelial cell line BEAS-2B and the LUSC cell lines. Data are presented as the mean ± SD from five independent experiments and were analyzed using an unpaired t-test or a two-way ANOVA followed by a Tukey's post-hoc multiple comparison analysis. **P<0.01, ***P<0.001, ****P<0.0001. HP, haptoglobin; LUSC, lung squamous cell carcinoma; TPM, transcripts per million; ns, not significant.

obtained (23) and analyzed the correlation between *HP* and characteristic genes of M2 macrophages. The results showed significant associations between *HP* and marker genes of M2 macrophages, such as *ACP5*, *AIF1* and *C3AR1*, with a Pearson correlation of 0.30 ($P=8.16x10^{-12}$), 0.28 ($P=8.15x10^{-11}$), and 0.21 ($P=1.37x10^{-6}$), respectively. These results demonstrated a positive correlation between *HP* gene expression and the abundance of M2 macrophages.

It was next investigated whether the overexpression of HP in LUSC cells induced ferroptosis in M2 macrophages. THP-1 cells were differentiated into M2 macrophages, as confirmed by flow cytometry demonstrating a $CD206^{+}CD163^{+}$ phenotype in ~80% of cells (Fig. 5A). Subsequently, NCI-H226 and NCI-H520 cells were transfected with lentivirus LV-*HP* or LV-Ctrl, and the CM was collected. M2 macrophages were exposed to the CM with or without Hb added for 24 h to assess induction of ferroptosis, marked by enhanced membrane permeability attributed to iron-dependent lipid peroxidation. The LDH release assay revealed that the LDH levels were not significantly altered in the supernatant of M2 macrophages exposed to CM from LV-*HP*-transfected tumor cells, LV-Ctrl-transfected cells and LV-Ctrl-transfected cells with Hb (LV-Ctrl/Hb) (Fig. 5B). Conversely, M2 macrophages cultured in CM from LV-*HP* with Hb (LV-*HP*/Hb) exhibited a significant increase in LDH release levels compared with that of the other three groups. Flow cytometry analysis of 7-AAD-positive cells indicated no statistically significant variances among the LV-Ctrl, LV-Ctrl/Hb and LV-*HP* groups, but a significantly higher percentage of 7-AAD-positive cells in the LV-*HP*/Hb group (Fig. 5C). Intracellular Fe^{2+} and lipid peroxide levels in M2 macrophages, measured using FerroOrange (Fig. 5D) and C11-BODIPY respectively (Fig. 5E), showed no significant differences among the LV-Ctrl, LV-Ctrl/Hb and LV-*HP* groups. However, the LV-*HP*/Hb group demonstrated a significantly higher fluorescence intensity for both markers, indicating increased free Fe^{2+} (Fig. 5D) and lipid peroxide (Fig. 5E) levels. Transmission electron microscopy showed ferroptotic characteristics in M2 macrophages from the LV-*HP*/Hb group, such as decreased mitochondrial size, increased mitochondrial membrane density and a reduction in mitochondrial cristae, with no similar morphological alterations observed in the other three groups (Fig. 5F). Taken together, these findings suggest

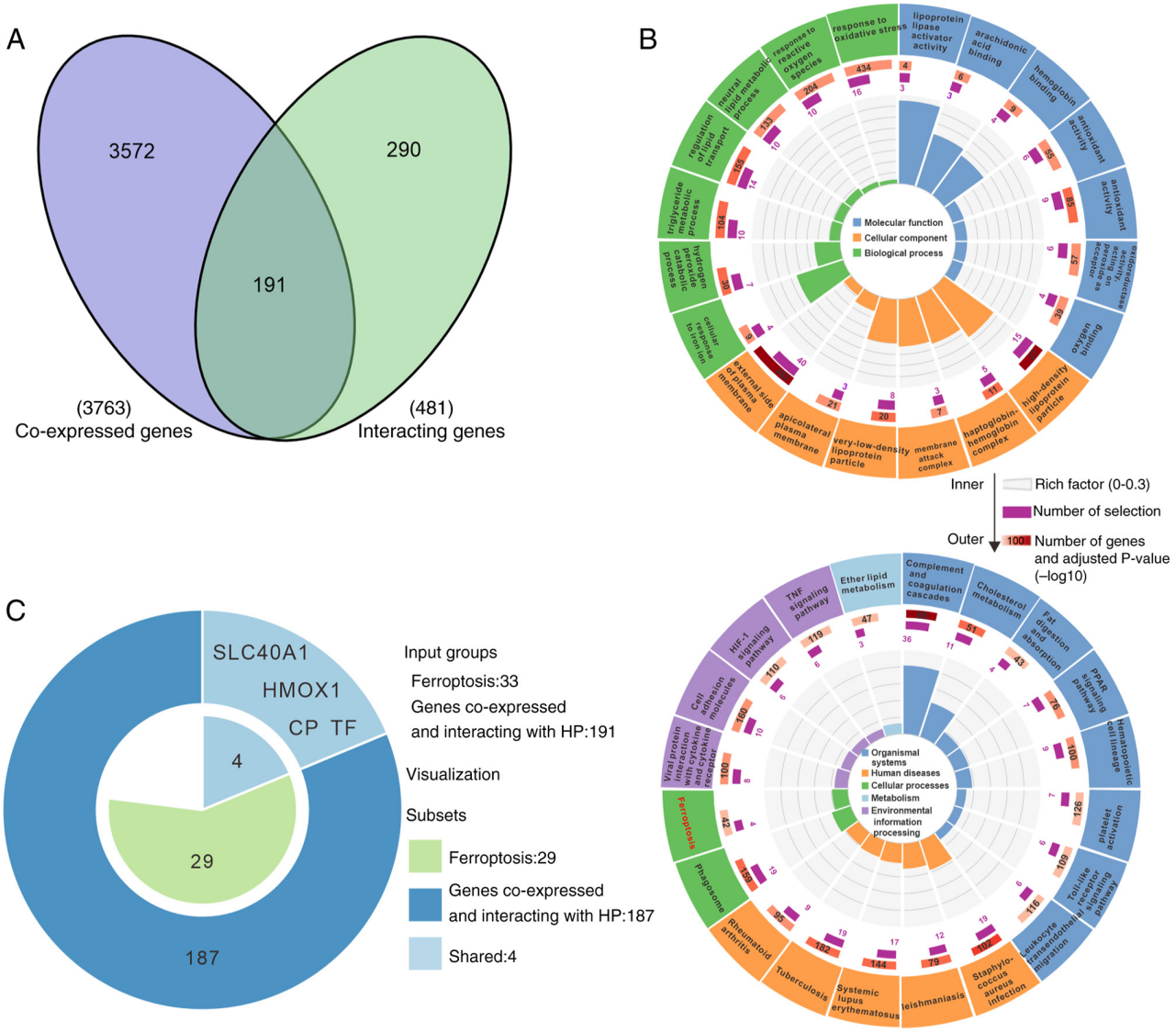

Figure 3. *HP* enrichment in LUSC suggests potential involvement in the ferroptosis signaling pathway. (A) In TCGA samples from the LinkedOmics database, 3,763 *HP*-associated genes were identified (FDR threshold <0.001), along with 481 genes interacting with *HP* sourced from the STRING database. An intersection analysis of the 3,763 *HP*-associated genes and the 481 *HP*-interacting genes yielded 191 overlapping genes. (B) The 191 genes associated with *HP* interactions were subjected to GO enrichment analysis and KEGG pathway enrichment analysis using R, followed by the generation of enrichment circle plots using OmicShare tools. The GO enrichment circle plot displayed seven biological processes, six cellular components and seven molecular function entries (upper); the KEGG enrichment circle plot showed a total of 20 entries (bottom). (C) The keyword 'Ferroptosis' was used to search the KEGG database, resulting in the retrieval of 33 genes relevant to ferroptosis. An intersection analysis of the 33 ferroptosis-related genes with the 191 genes from (A) identified four intersecting genes: *HMOX1*, *SLC40A1*, *CP* and *TF*. *HP*, haptoglobin; LUSC, lung squamous cell carcinoma; GO, Gene Ontology; KEGG, Kyoto Encyclopedia of Genes and Genomes; FDR, false-discovery rate.

the CM from lung squamous carcinoma cells overexpressing HP effectively triggered ferroptosis in M2 macrophages in the presence of Hb.

HP promotes ferroptosis in M2 macrophages by inducing intracellular Fe^{2+} generation via a CD163/HO-1 signaling pathway. To investigate the role of HP in intracellular Fe^{2+} generation and ferroptosis induction in M2 macrophages, NCI-H226 and NCI-H520 cells were transfected with LV-HP or LV-Ctrl. The resulting supernatants were used as CM. M2 macrophages were exposed to different combinations of CM, Hb and an anti-CD163 antibody. After 24 h, heme and HO-1 protein levels were measured, along with markers of ferroptosis. Spectrophotometry analysis showed that in the absence of HP, there was no significant difference in heme levels between the LV-Ctrl/Hb and LV-Ctrl/Hb/anti-CD163 groups. However, in the presence of HP, heme levels in the LV-*HP*/Hb/anti-CD163 group were significantly decreased when compared with that of the LV-*HP*/Hb group (Fig. 6A). These findings suggested that blocking CD163 receptors with an anti-CD163 antibody impeded Hb entry into M2 macrophages, thereby reducing intracellular heme production.

The results of flow cytometry analysis of intracellular HO-1 protein levels were similar to those of heme detection (27,31). There was no significant difference in HO-1 levels between the LV-Ctrl/Hb and LV-Ctrl/Hb/anti-CD163 groups; however, the HO-1 levels in the LV-*HP*/Hb/anti-CD163 group were significantly lower compared with those in the LV-*HP*/Hb group

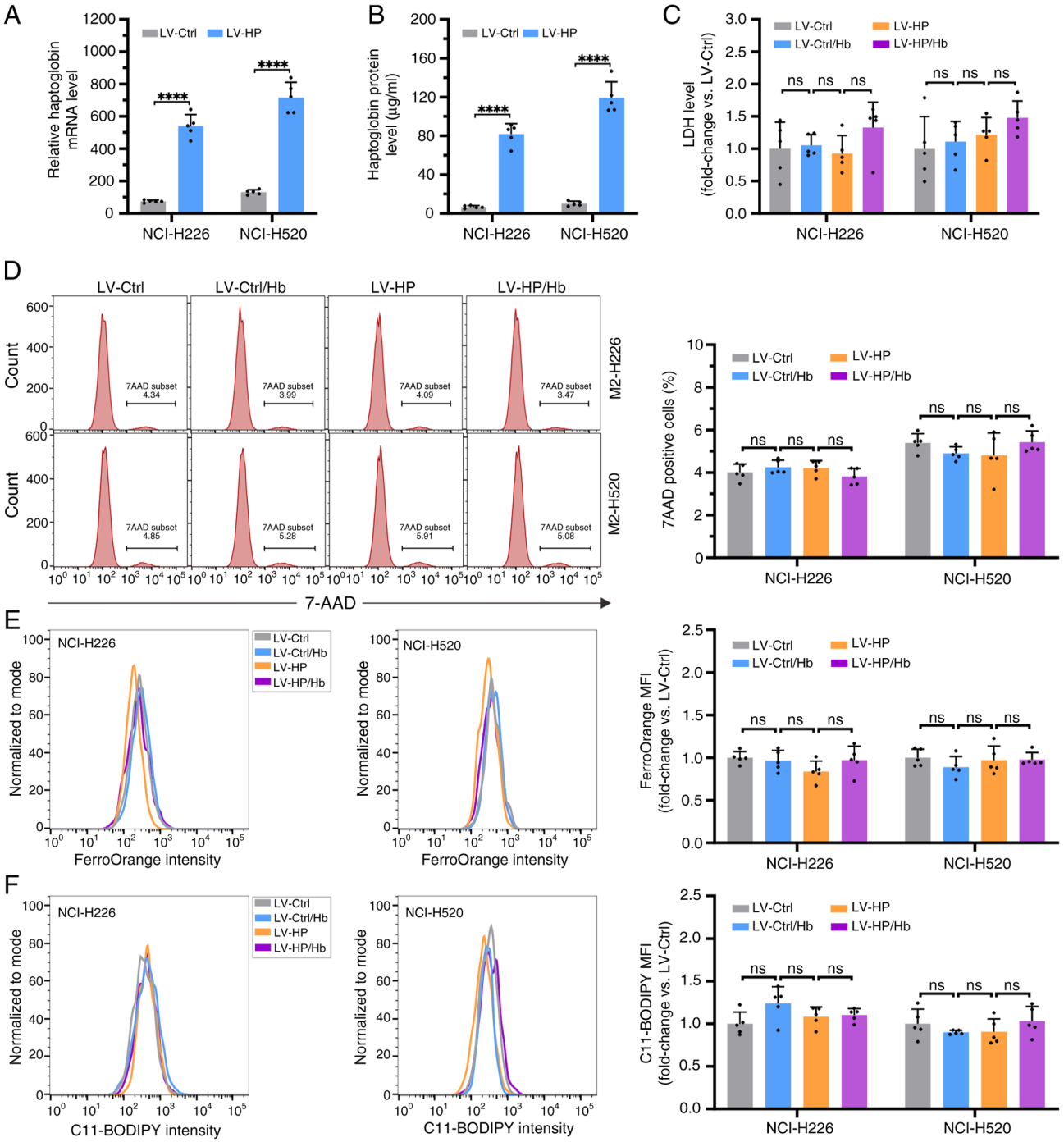

Figure 4. Overexpression of HP in LUSC cells does not induce ferroptosis in LUSC cells. (A and B) NCI-H226 and NCI-H520 cells were infected with LV-*HP* or LV-Ctrl. After 72 h of infection, cells and culture supernatants were collected for analysis of *HP* (A) mRNA and (B) protein levels by RT-PCR and ELISA, respectively. (C) NCI-H226 and NCI-H520 cells infected with LV-*HP* or LV-Ctrl were cultured with or without Hb (30 μg/ml) for 24 h. Culture supernatants were collected and LDH release was measured. (D) Cells were analyzed via flow cytometry to determine the percentage of 7-AAD-positive cells in NCI-H226 and NCI-H520 cells. (E and F) The mean fluorescence intensity of (E) FerroOrange (Fe^{2+}) and (F) C11-BODIPY (lipid peroxide) was measured using flow cytometry. Data are presented as the mean ± SD from five independent experiments and were analyzed using an unpaired t-test or a two-way ANOVA followed by a Tukey's post-hoc multiple comparison analysis. ****P<0.0001. ns, not significant; HP, haptoglobin; Hb, hemoglobin; LDH, lactate dehydrogenase; 7-AAD, 7-aminoactinomycin D.

(Fig. 6B), consistent with previous research findings (27,31). To confirm the impact of CD163, HO-1, and Fe^{2+} on M2 macrophage ferroptosis, M2 macrophages were treated with an anti-CD163 antibody, the HO-1 inhibitor SnPPIX or the Fe^{2+} chelator DFO. Ferroptosis markers were then assessed using flow cytometry, including 7-AAD-positive membrane-permeable dead cells, Fe^{2+} and lipid peroxide. In the absence of HP, the addition of the anti-CD163 antibody did not affect 7-AAD-positive death cells, Fe^{2+} levels and lipid peroxide in the LV-Ctrl/Hb and LV-Ctrl/Hb/anti-CD163 groups (Fig. 6C-E). However, in the presence of both HP and Hb, treatment with the anti-CD163 antibody significantly reduced the levels of 7-AAD-positive dead cells, Fe^{2+} and lipid peroxide compared to the groups without antibody treatment (Fig. 6C-E). Similar results were

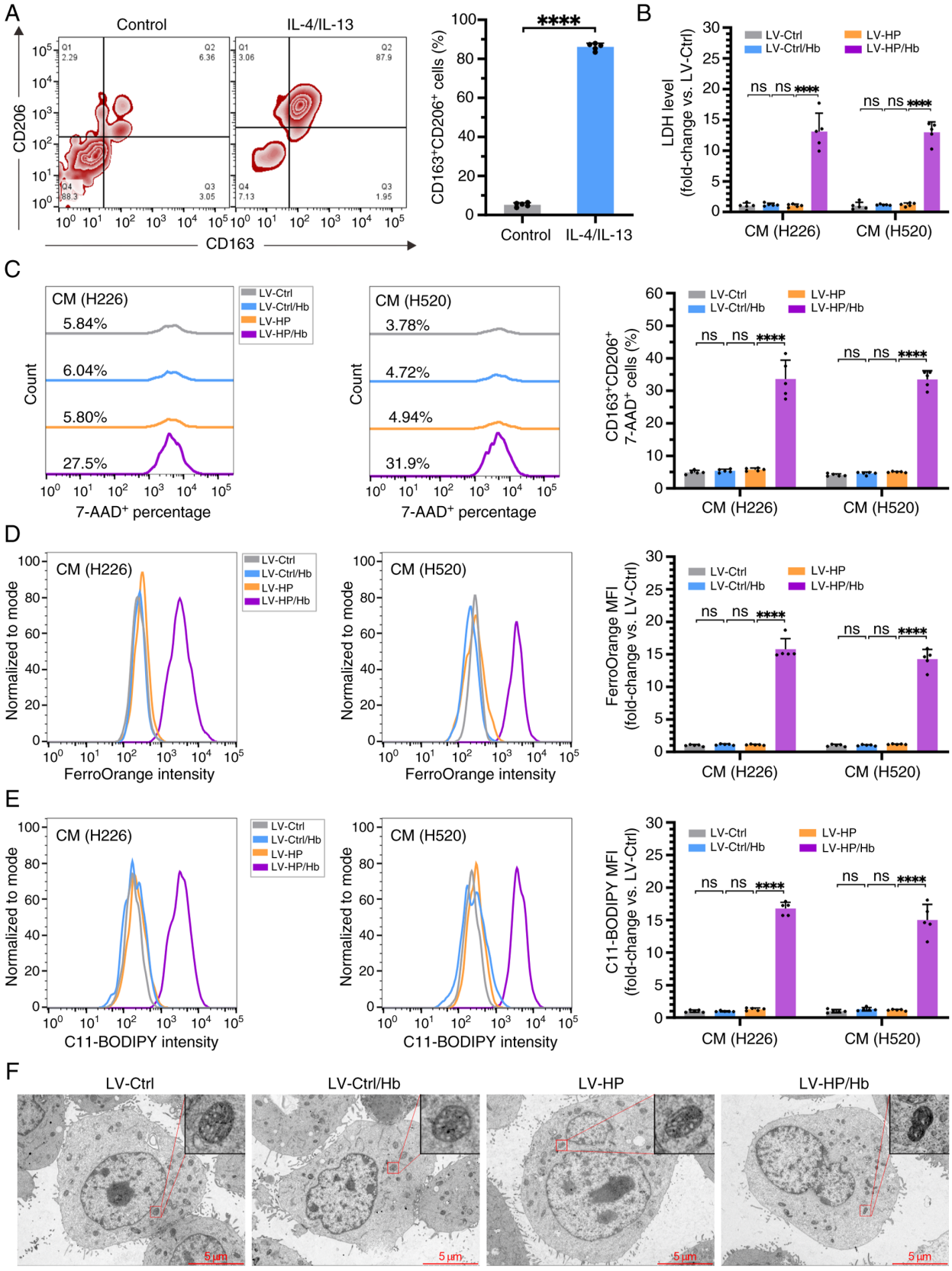

Figure 5. CM from LUSC cells overexpressing HP leads to ferroptosis in M2 macrophages. (A) THP-1 cells were differentiated into macrophages by treating them with 150 nM PMA for 24 h, followed by culture in fresh RPMI-1640 for 24 h. The macrophages were polarized into M2 macrophages by incubating with IL-4 (20 ng/ml) and IL-13 (20 ng/ml) for 24 h. Flow cytometry was then performed to identify $CD163^{+}CD206^{+}$ M2 macrophages. (B) M2 macrophages were cultured with the CM from NCI-H226 and NCI-H520 cells infected with LV-*HP* or LV-Ctrl in the presence or absence of Hb for 24 h. LDH release was analyzed by ELISA. Treated M2 macrophages were treated as in (B) and flow cytometry was used to detect the proportion of (C) 7-AAD positive cells, as well as the mean fluorescence intensity of (D) FerroOrange and (E) C11-BODIPY. (F) Treated M2 macrophages were observed using transmission electron microscopy. Scale bar, 5 μm. Data are presented as the mean ± SD from five independent experiments and were analyzed using an unpaired t-test or a two-way ANOVA followed by a Tukey's post-hoc multiple comparison analysis. ****P<0.0001. ns, not significant; CM, conditioned media; LUSC, lung squamous cell carcinoma; LDH, lactate dehydrogenase; 7-AAD, 7-aminoactinomycin D; HP, haptoglobin.

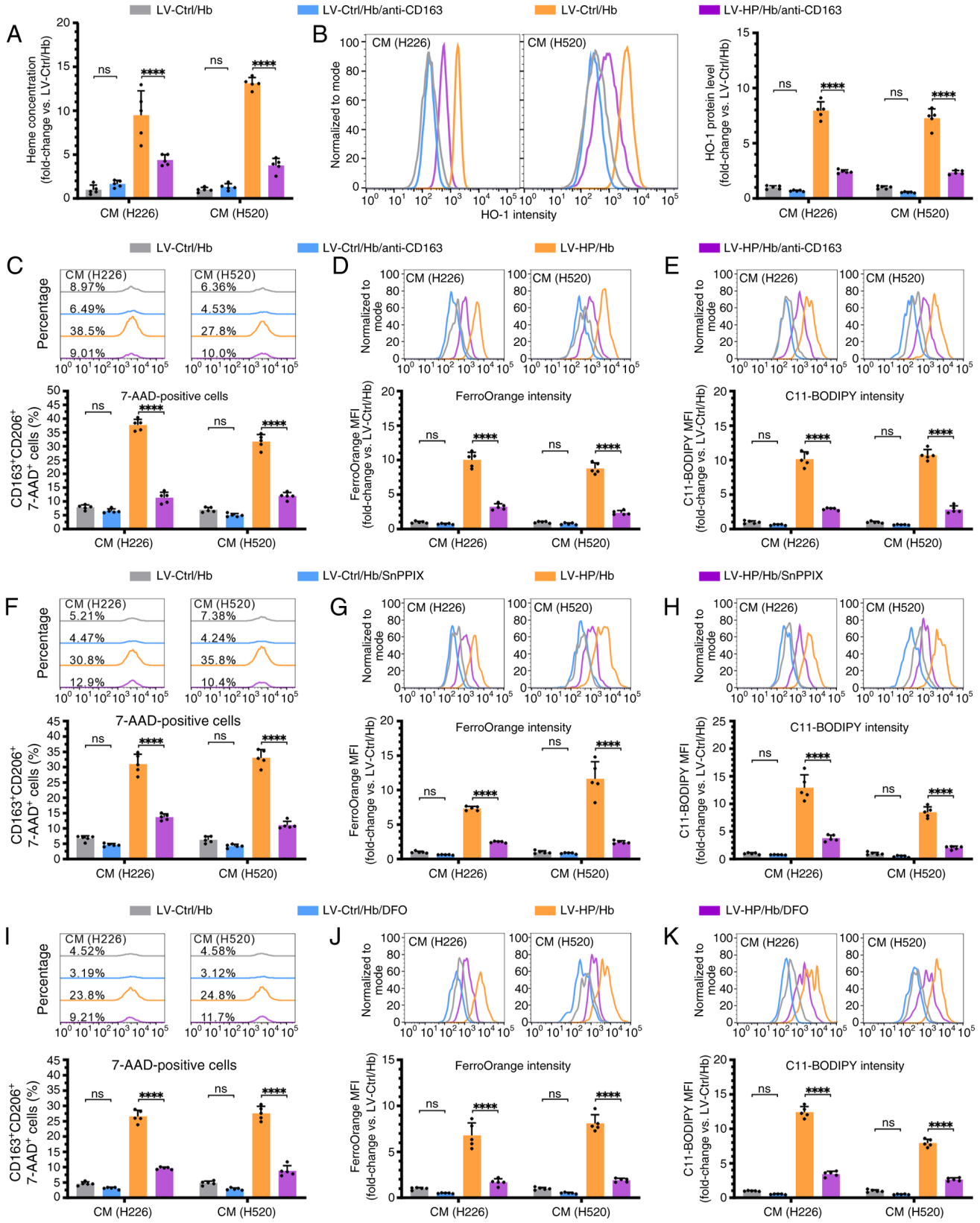

Figure 6. HP promotes ferroptosis in M2 macrophage by inducing intracellular Fe^{2+} generation via the CD163/HO-1 signaling pathway. (A and B) M2 macrophages were cultured with CM from NCI-H226 and NCI-H520 cells infected with LV-*HP* or LV-Ctrl, in the presence of Hb and an anti-CD163 antibody. The heme levels in M2 macrophages were measured using (A) spectrophotometry and (B) HO-1 protein expression levels were examined using flow cytometry. (C) M2 macrophages were co-cultured with CM containing Hb, with or without the addition of an anti-CD163 antibody, the HO-1 inhibitor SnPPIX, or the Fe^{2+} chelator DFO for 24 h. (D) Following treatment with the anti-CD163 antibody, the percentage of 7-AAD$^+$ cells, and the mean fluorescence intensity of FerroOrange and (E) C11-BODIPY were analyzed by flow cytometry. After SnPPIX treatment, (F) 7-AAD$^+$ cells, (G) FerroOrange intensity (H) and C11-BODIPY intensity were assessed. Following DFO treatment, (I) 7-AAD$^+$ cells, (J) FerroOrange intensity, and (K) C11-BODIPY intensity were measured. Data are presented as the mean ± SD from five independent experiments and were analyzed using an unpaired t-test or a two-way ANOVA followed by a Tukey's post-hoc multiple comparison analysis. ****P<0.0001. HP, haptoglobin; CM, conditioned media; Hb, hemoglobin; 7-AAD, 7-aminoactinomycin D; HO-1, heme oxygenase-1; DFO, deferoxamine.

found in the corresponding M2 macrophages treated with SnPPIX (Fig. 6F-H) and DFO (Fig. 6I-K). Taken together, these findings indicated that HP promoted ferroptosis in M2 macrophages by inducing intracellular Fe^{2+} generation through the CD163/HO-1 signaling pathway.

Discussion

LUSC remains a leading cause of cancer-related mortality, with the majority of patients being diagnosed with advanced-stage disease, resulting in high mortality rates (32). Due to the lack of targeted therapies for LUSC, treatment options for patients with advanced-stage disease are extremely limited. Currently, immune checkpoint inhibitors have emerged as a relatively successful therapeutic strategy for patients with LUSC (5). However, the lower response rates and severe adverse reactions have hindered the application of immunotherapy in these patients (6). Therefore, there is an urgent need to explore novel strategies for the management of LUSC. In the present study, the HP gene was identified as a hub gene in LUSC via bioinformatics analysis. It was demonstrated that HP expression levels were lower in LUSC cells compared with that of normal lung tissue cells, and were significantly associated with patient prognosis. Further bioinformatics analysis suggested that HP enrichment in LUSC indicated potential involvement in the ferroptosis signaling pathway. Mechanistic investigations using *in vitro* cell experiments revealed that overexpression of HP in LUSC cells did not induce ferroptosis in the cells themselves, but rather promoted intracellular Fe^{2+} accumulation in M2 macrophages via the CD163/HO-1 signaling pathway, ultimately inducing ferroptosis in M2 macrophages. These findings suggest a potential mechanism by which LUSC downregulates HP expression to inhibit M2 macrophage ferroptosis.

APPs are critical regulatory proteins that modulate their expression in response to inflammatory processes (33). Emerging research indicates that inflammatory mechanisms significantly contribute to tumor development, with APPs serving a pivotal role in tumor cell migration, invasion and anti-apoptotic inflammatory responses (9), suggesting their potential as tumor growth inhibitors. At present, the APP gene A2M has been identified as a potential therapeutic target for NSCLC (13). However, the therapeutic implications of other APPs in tumor management, particularly in LUSC, remain unexplored. The present study initially identified a total of 107 APP genes from the GeneCards database. To focus on APP genes affecting LUSC growth, the overlap between these 107 APP genes and DEGs in LUSC were analyzed using protein-protein interaction and cytoHubba algorithms. As a result, 8 APP genes were pinpointed as hub genes for LUSC. Subsequent survival analysis of these 8 hub genes revealed that only HP and A2M were significant for the prognosis of patients with LUSC. Given that A2M has been reported as a potential therapeutic target for NSCLC, HP was selected to explore its role in inducing ferroptosis in LUSC. Further bioinformatics analysis and *in vitro* cell experiments demonstrated a decreased expression of HP in LUSC tumor tissues and various cell lines (NCI-H226, NCI-H520, NCI-H1703 and NCI-H2170). Enrichment analysis suggested that HP is potentially involved in the ferroptosis signaling pathway in LUSC. Consequently, lentiviral vectors were employed to overexpress HP in LUSC cells, followed by a series of *in vitro* cellular experiments. The results indicated that overexpression of HP in LUSC cells did not directly trigger ferroptosis, as evidenced by the lack of significant differences in LDH release, the frequency of 7-AAD-positive cells, Fe^{2+} levels and lipid peroxidation across the LV-Ctrl, LV-HP, LV-Ctrl/Hb and LV-HP/Hb groups. Instead, the CM from HP-overexpressing LUSC cells in the presence of Hb (LV-HP/Hb group) increased ferroptosis in M2 macrophages compared with that of the three control groups. This was supported by an increase in LDH release, the frequency of 7-AAD-positive cells, Fe^{2+} levels, lipid peroxidation and mitochondrial abnormalities observed under transmission electron microscopy. These findings indicated that overexpression of HP in *in vitro* cell models of LUSC cells effectively induce M2 macrophage ferroptosis in the presence of Hb.

Ferroptosis is a form of cell death characterized by increased iron levels, which drive the generation of numerous lipid peroxides, leading to increased cell membrane permeability and ultimately cell death (28). Iron metabolism serve a crucial regulatory role in the regulation of ferroptosis. Previous studies have demonstrated that *HP*, *HMOX1*, *SLC40A1*, *CP* and *TF* facilitate the retrieval of iron from free Hb via M2 macrophages (29,30). M2 macrophages serve a crucial regulatory role in hemoglobin-iron recycling by internalizing the HP/Hb complex via CD163. HP binds to Hb from damaged red blood cells and enters M2 macrophages via CD163, where the Hb moiety is catabolized to heme within lysosomes (29,34). HO-1, encoded by *HMOX1*, converts heme to free iron (Fe^{2+}) (29). Ferroportin, produced by *SLC40A1*, transports most free iron extracellularly (29). Ceruloplasmin, encoded by *CP*, oxidizes extracellular iron to Fe^{3+}, which subsequently binds to transferrin, encoded by *TF*, and is internalized by iron-requiring cells (30). This suggests that the ferroptosis mechanism involving *HP* may occur in M2 macrophages. M2 macrophages are the predominant tumor-associated macrophages in the tumor microenvironment, serving a key role in promoting tumor growth through interactions with the tumor immune microenvironment (35,36). It was previously reported that patients with high levels of M2 macrophage infiltration in LUSC tend to have a poorer prognosis (37). Therefore, targeting M2 macrophages represents a potential strategy for cancer management. The present study demonstrated a significant amount of Hp-Hb complexes promote the generation of Fe^{2+} within M2 macrophages via the CD163/HO-1 pathway, reflecting the iron uptake process by M2 macrophages. While the iron metabolism of M2 macrophages involves both iron uptake and iron efflux, the specific pathway of iron efflux was not elucidated in the present study. The regulatory mechanisms of this process may exhibit specificity in LUSC, thereby limiting the direct extrapolation of the functional changes identified in the present study to other cancer types. Therefore, future research needs to systematically map the complete iron metabolism profile of M2 macrophages in LUSC, particularly focusing on their iron efflux pathway.

The present *in vitro* experiments showed that overexpression of *HP* in LUSC induced M2 macrophage ferroptosis, indicating its potential in eliminating immune-suppressive cells. However, prognosis and immune infiltration analysis using patient data from the TCGA database for LUSC revealed

that patients with LUSC with high HP expression have worse outcomes compared with those with low HP expression, with significantly higher levels of M2 macrophage infiltration, a trend consistent with previous reports associating elevated serum HP levels with adverse prognosis in NSCLC (38). These findings suggested that the role of *HP* in the complex tumor microenvironment *in vivo* is more intricate than a singular mechanism observed *in vitro*. It could be considered that in a complete tumor ecosystem, the direct cytotoxic effect of *HP* on M2 macrophages may trigger a more intense compensatory immune reshaping. The process of remodeling may involve the generation of ROS from ferroptosis, potentially enhancing the sustained recruitment of tumor-associated macrophages and their differentiation into M2 macrophages under the influence of local tumor microenvironment factors (39), thereby reinforcing the immune-suppressive milieu and ultimately associating with malignant progression and poor prognosis of tumors. *HP* may be a key player in the tumor immune microenvironment, operating not through a simple linear clearance mechanism but embedded within a dynamic network of regulation. Future research should further validate the existence of this 'compensatory recruitment' in *in vivo* models and explore the feasibility of targeting *HP* as a therapeutic approach. For instance, concurrent targeting of the *HP* pathway and the key chemokine receptor CCR2 (40) for monocyte recruitment may synergistically disrupt this detrimental immune homeostasis, offering new avenues for immune combination therapy for LUSC.

However, there were still several limitations in the present study. It was found through bioinformatics that low HP expression in LUSC is negatively correlated with patient prognosis, and four ferroptosis-related genes (*HMOX1*, *SLC40A1*, *CP* and *TF*) were identified as being associated with and interacting with *HP*. Among these, three genes (*HMOX1*, *SLC40A1* and *TF*) showed relatively weak correlations with *HP* ($r<0.3$), warranting further validation of their roles in HP-mediated ferroptosis. *In vitro* cell experiments also showed that high expression of HP in LUSC cells promoted M2 macrophage ferroptosis via the hemoglobin-dependent CD163/HO-1 pathway, thereby indirectly validating that low expression of HP in LUSC cells may inhibit M2 macrophage ferroptosis. However, this mechanism has not been further validated *in vivo*, and the relationship or mechanism between M2 macrophage ferroptosis and LUSC prognosis has not been comprehensively studied. The potential reason for this is that, in contrast to human HP, mouse HP does not promote high-affinity binding of mouse Hb to CD163 (41), which limits the ability to validate the function of the identified hemoglobin-dependent CD163/HO-1 pathway *in vivo* using mouse tumor models. Additionally, due to limitations in available resources, clinical samples for *in vivo* validation could not be conducted. Furthermore, the simplification of *in vitro* experimental systems fails to replicate the complex tumor microenvironment and its compensatory feedback networks *in vivo*, making single intervention strategies ineffective *in vivo*. Even with sufficient clinical samples from patients with LUSC, verification of the mechanism of downregulating haptoglobin expression to inhibit M2 macrophage ferroptosis via the hemoglobin-dependent CD163/HO-1 pathway remains challenging. Therefore, future studies should utilize appropriate *in vivo* models and systematic combined interventions to investigate whether LUSC regulates the tumor immune microenvironment by downregulating HP expression to inhibit M2 macrophage ferroptosis. In summary, the present study demonstrated that the *HP* gene served a central role in LUSC. *HP* was significantly downregulated in LUSC and was associated with patient prognosis. Overexpression of HP in LUSC cells led to exogenous Hb binding, triggering M2 macrophage ferroptosis via the CD163/HO-1 pathway. These findings suggested that LUSC may decrease *HP* expression to modulate ferroptosis in M2 macrophages, which may provide a promising direction for future research on LUSC.

Acknowledgements

Not applicable.

Funding

The present study was funded by the National Natural Science Foundation of China (grant no. 32460190) and the Hainan Provincial Natural Science Foundation (grant no. ZDKJ202003).

Availability of data and materials

The datasets used and/or analyzed during the present study are available from the corresponding author on reasonable request.

Authors' contributions

FYH and GHT designed the study, and drafted and revised the manuscript. WX, YYL and FYH performed the experiments and analyzed the data. FYH and GHT oversaw the manuscript and gave approval for the final submitted version. FYH and WX confirm the authenticity of all the raw data. All authors have read and approved the final manuscript.

Ethics approval and consent to participate

Not applicable.

Patient consent for publication

Not applicable.

Competing interests

The authors declare that they have no competing interests.

References

1. Brody H: Lung cancer. Nature 587 (Suppl 1): S7, 2020.
2. Herbst RS, Morgensztern D and Boshoff C: The biology and management of non-small cell lung cancer. Nature 553: 446-454, 2018.
3. Siegel RL, Giaquinto AN and Jemal A: Cancer statistics, 2024. CA Cancer J Clin 74: 12-49, 2024.
4. Bonomi PD, Gandara D, Hirsch FR, Kerr KM, Obasaju C, Paz-Ares L, Bellomo C, Bradley JD, Bunn PA Jr, Culligan M, *et al*: Predictive biomarkers for response to EGFR-directed monoclonal antibodies for advanced squamous cell lung cancer. Ann Oncol 29: 1701-1709, 2018.

5. Herbst RS, Baas P, Kim DW, Felip E, Pérez-Gracia JL, Han JY, Molina J, Kim JH, Arvis CD, Ahn MJ, *et al*: Pembrolizumab versus docetaxel for previously treated, PD-L1-positive, advanced non-small-cell lung cancer (KEYNOTE-010): A randomised controlled trial. Lancet 387: 1540-1550, 2016.
6. Karachaliou N, Fernandez-Bruno M and Rosell R: Strategies for first-line immunotherapy in squamous cell lung cancer: Are combinations a game changer? Transl Lung Cancer Res 7 (Suppl 3): S198-S201, 2018.
7. Marusyk A, Janiszewska M and Polyak K: Intratumor heterogeneity: The Rosetta stone of therapy resistance. Cancer Cell 37: 471-484, 2020.
8. Cray C, Zaias J and Altman NH: Acute phase response in animals: A review. Comp Med 59: 517-526, 2009.
9. Nickoloff BJ, Ben-Neriah Y and Pikarsky E: Inflammation and cancer: Is the link as simple as we think? J Invest Dermatol 124: 1275-1284, 2005.
10. Chen L, Wei WH, Sun J, Sun BC and Deng R: Cordycepin enhances anti-tumor immunity in breast cancer by enhanceing ALB expression. Heliyon 10: e29903, 2024.
11. Zhang GR, Liu XY, Sun ZY, Feng XN, Wang HY, Hao J and Zhang XL: A2M is a potential core gene in intrahepatic cholangiocarcinoma. BMC Cancer 22: 5, 2022.
12. Zheng TZ, Zheng ZW, Zhou HX, Guo YQ and Li SK: The multifaceted roles of COL4A4 in lung adenocarcinoma: An integrated bioinformatics and experimental study. Comput Biol Med 170: 107896, 2024.
13. Zhang NN: Screening and identification of diagnostic and therapeutic targets of NSCLC and exploring the expression and clinical significance of A2M in NSCLC. China National Knowledge Infrastructure, Lanzhou University, 2019.
14. Lei G, Zhuang L and Gan BY: Targeting ferroptosis as a vulnerability in cancer. Nat Rev Cancer 22: 381-396, 2022.
15. Stockwell BR, Friedmann Angeli JP, Bayir H, Bush AI, Conrad M, Dixon SJ, Fulda S, Gascón S, Hatzios SK, Kagan VE, *et al*: Ferroptosis: A regulated cell death nexus linking metabolism, redox biology, and disease. Cell 171: 273-285, 2017.
16. Tang D, Kroemer G and Kang R: Ferroptosis in hepatocellular carcinoma: From bench to bedside. Hepatology 80: 721-739, 2024.
17. Lei Y, Jiang S, Kong C, Pang P and Shan H: Ferroptosis: Therapeutic potential and strategies in Non-Small cell lung cancer. Biology (Basel) 14: 545, 2025.
18. Chen X, Comish PB, Tang DL and Kang R: Characteristics and biomarkers of ferroptosis. Front Cell Dev Biol 9: 637162, 2021.
19. Koppula P, Zhuang L and Gan BY: Cytochrome P450 reductase (POR) as a ferroptosis fuel. Protein cell 12: 675-679, 2021.
20. Chen X, Yu CH, Kang R and Tang DL: Iron metabolism in ferroptosis. Front Cell Dev Biol 8: 590226, 2020.
21. di Masi A, De Simone G, Ciaccio C, D'Orso S, Coletta M and Ascenzi P: Haptoglobin: From hemoglobin scavenging to human health. Mol Aspects Med 73: 100851, 2020.
22. Kristiansen M, Graversen JH, Jacobsen C, Sonne O, Hoffman HJ, Law SK and Moestrup SK: Identification of the haemoglobin scavenger receptor. Nature 409: 198-201, 2001.
23. Newman AM, Liu CL, Green MR, Gentles AJ, Feng WG, Xu Y, Hoang CD, Diehn M and Alizadeh AA: Robust enumeration of cell subsets from tissue expression profiles. Nat Methods 12: 453-457, 2015.
24. Kawase A, Takashima O, Tanaka S, Shimada H and Iwaki M: Diclofenac-induced cytotoxicity in direct and indirect co-culture of HepG2 cells with differentiated THP-1 cells. Int J Mol Sci 23: 8660, 2022.
25. Livak KJ and Schmittgen TD: Analysis of relative gene expression data using real-time quantitative PCR and the 2(-Delta Delta C(T)) method. Methods 25: 402-408, 2001.
26. Huang FY, Dai SZ, Xu WT, Xiong W, Sun Y, Huang YH, Wang JY, Lin YY, Chen H, Tan GH and Zheng WP: 3'-epi-12β-hydroxyfroside-mediated autophagy degradation of RIPK1/RIPK3 necrosomes leads to anergy of immunogenic cell death in triple-negative breast cancer cells. Pharmacol Res 187: 106613, 2023.
27. Delaby C, Pilard N, Puy H and Canonne-Hergaux F: Sequential regulation of ferroportin expression after erythrophagocytosis in murine macrophages: Early mRNA induction by haem, followed by iron-dependent protein expression. Biochem J 411: 123-131, 2008.
28. Li SX and Huang Y: Ferroptosis: An iron-dependent cell death form linking metabolism, diseases, immune cell and targeted therapy. Clin Transl Oncol 24: 1-12, 2022.
29. Cairo G, Recalcati S, Mantovani A and Locati M: Iron trafficking and metabolism in macrophages: Contribution to the polarized phenotype. Trends Immunol 32: 241-247, 2011.
30. Fonseca Ó, Ramos AS, Gomes LTS, Gomes MS and Moreira AC: New perspectives on circulating ferritin: Its role in health and disease. Molecules 28: 7707, 2023.
31. Alam J, Stewart D, Touchard C, Boinapally S, Choi AM and Cook JL: Nrf2, a Cap'n'Collar transcription factor, regulates induction of the heme oxygenase-1 gene. J Biol Chem 274: 26071-26078, 1999.
32. Lau SCM, Pan YW, Velcheti V and Wong KK: Squamous cell lung cancer: Current landscape and future therapeutic options. Cancer Cell 40: 1279-1293, 2022.
33. Kushner I and Mackiewicz A: Acute phase proteins as disease markers. Dis Markers 5: 1-11, 1987.
34. Thomsen JH, Etzerodt A, Svendsen P and Moestrup SK: The haptoglobin-CD163-heme oxygenase-1 pathway for hemoglobin scavenging. Oxid Med Cell Longev 2013: 523652, 2013.
35. Dai EY, Han L, Liu J, Xie YC, Kroemer G, Klionsky DJ, Zeh HJ, Kang R, Wang J and Tang DL: Autophagy-dependent ferroptosis drives tumor-associated macrophage polarization via release and uptake of oncogenic KRAS protein. Autophagy 16: 2069-2083, 2020.
36. Qian Y, Qiao S, Dai YF, Xu GQ, Dai BL, Lu LS, Yu X, Luo QM and Zhang ZH: Molecular-Targeted immunotherapeutic strategy for melanoma via Dual-targeting nanoparticles delivering small interfering RNA to Tumor-associated macrophages. ACS Nano 11: 9536-9549, 2017.
37. Han YS and Li YX: Comprehensive exploration of M2 macrophages and its related genes for predicting clinical outcomes and drug sensitivity in lung squamous cell carcinoma. J Oncol 2022: 1163924, 2022.
38. Lu JJ, Wang YH, Yan MS, Feng PN, Yuan LJ, Cai YS, Xia X, Liu M, Luo JM and Li LS: High serum haptoglobin level is associated with tumor progression and predicts poor prognosis in non-small cell lung cancer. Oncotarget 7: 41758-41766, 2016.
39. Liang XS, Weng JD, You ZY, Wang Y, Wen J, Xia ZW, Huang SR, Luo P and Cheng Q: Oxidative stress in cancer: From tumor and microenvironment remodeling to therapeutic frontiers. Mol Cancer 24: 219, 2025.
40. Muscat S, Nichols AEC, Gira E and Loiselle AE: CCR2 is expressed by tendon resident macrophage and T cells, while CCR2 deficiency impairs tendon healing via blunted involvement of tendon-resident and circulating monocytes/macrophages. FASEB J 36: e22607, 2022.
41. Etzerodt A, Kjolby M, Nielsen MJ, Maniecki M, Svendsen P and Moestrup SK: Plasma clearance of hemoglobin and haptoglobin in mice and effect of CD163 gene targeting disruption. Antioxid Redox Signal 18: 2254-2263, 2013.